

A combination of a Drickamer anvil apparatus and monochromatic X-rays for stress and strain measurements under high pressure

Norimasa Nishiyama,^{a*} Yanbin Wang,^b Tetsuo Irifune,^a Takeshi Sanehira,^b Mark L. Rivers,^b Steve R. Sutton^b and David Cookson^b

^aGeodynamics Research Center, Ehime University, 2-5 Bunkyo-cho, Matsuyama 790-8577, Japan, and ^bCenter for Advanced Radiation Sources, The University of Chicago, 5640 South Ellis Avenue, Chicago, IL 60637, USA. E-mail: nishiyama@sci.ehime-u.ac.jp

A modified Drickamer anvil apparatus has been developed to combine with monochromatic synchrotron radiation for high-pressure X-ray diffraction and radiography in the GSECARS bending-magnet station, 13-BM-D, at the Advanced Photon Source, Argonne, USA. Using this experimental set-up, deformation experiments can be carried out at pressures in excess of 30 GPa at high temperatures. Differential stresses and total axial strains of polycrystalline platinum and Mg₂SiO₄ ringwoodite have been measured up to 32 GPa at room temperature using tungsten carbide anvils. The total axial strain of the platinum increases with pressure and reaches about 55% at the highest pressure. A test run using a composite sintered diamond anvil system was performed. The use of X-ray-transparent anvils enables the entire Debye rings to be observed up to 10° 2θ. With high-energy photons (65–70 keV), this allows a coverage in $Q (= 2\pi \sin \theta / \lambda)$ to about 3 Å⁻¹, thus making it possible to evaluate hydrostatic pressure and differential stress in crystalline minerals using diffraction. This, coupled with the ability to determine axial strain, allows deformation studies to be performed to pressures above 30 GPa.

© 2009 International Union of Crystallography
Printed in Singapore – all rights reserved

Keywords: high pressure; deformation; Drickamer apparatus; differential stress; strain.

1. Introduction

Diamond anvil cells (DACs) have been widely used for strength measurements under high pressure (e.g. Kinsland & Bassett, 1977; Meade & Jeanloz, 1988). Recently, radial X-ray diffraction has been used in DACs with synchrotron radiation to carry out stress measurements under high pressure (e.g. Mao *et al.*, 1998; Merkel *et al.*, 2007). This technique has also been used to determine active slip systems on deformation (e.g. Wenk *et al.*, 2000). Although the DAC has the advantage of measuring stress above 1 Mbar pressure (e.g. Duffy *et al.*, 1995), it is quite difficult to measure sample strain, which is another indispensable parameter for describing deformation, because samples in the DAC are very thin, *i.e.* they may be less than 10 µm under pressures above 10 GPa (Merkel *et al.*, 2002).

The Drickamer apparatus (e.g. Balchan & Drickamer, 1961) is an opposed-anvil device employing a containment cylinder which aligns the anvils and prevents gasket flow. This apparatus has also been used for stress and strength measurements. Funamori *et al.* (1994) applied the radial X-ray diffraction technique to the Drickamer apparatus using a white beam with two solid-state detectors in both vertical (parallel to the

compression direction) and horizontal directions (Yagi *et al.*, 1992) and measured the differential stress of sodium chloride under pressure. The sample volume in the Drickamer apparatus is much larger than that of the DAC. For example, Yagi *et al.* (1992) used the Drickamer apparatus with a culet diameter of 3 mm and the initial height of their sample was 1 mm (0.6 mm after compression). Therefore, the Drickamer apparatus has the potential to carry out stress and macroscopic strain measurements simultaneously under pressure because X-ray radiography techniques are readily available for measuring sample length under pressure (e.g. Wang *et al.*, 2003). In addition, Funamori & Yagi (1993) and Gotou *et al.* (2006) developed internal heating methods for the Drickamer apparatus, and they succeeded in generating simultaneous high pressure and temperature up to 36 GPa and 1900 K (Funamori & Yagi, 1993). Thus, the Drickamer apparatus has the potential to accomplish stress and strain measurements of deformed polycrystalline samples under high pressure and temperature conditions corresponding to the Earth's lower mantle.

We have developed a modified Drickamer apparatus for monochromatic X-ray diffraction and imaging to measure differential stress and macroscopic strain under high pressure

and room temperature. In this paper we present a detailed design of the Drickamer apparatus and the experimental set-up. We also report some examples of experimental results to show the methods of evaluating stress and strain under pressure in the Drickamer apparatus. High-temperature techniques are under development for future high pressure and temperature deformation studies.

2. Apparatus and experimental set-up

2.1. Anvils and containment ring

Figs. 1(a) and 1(b) show, respectively, a schematic three-dimensional illustration and a cross section of the Drickamer cell used in the present study. The cell consists of two tungsten carbide (WC) anvils (A) with ultra-micro grains (Fujilloy-TF05, Fuji Die Company) and a tool steel containment ring (B) to align the anvils. The inner diameter and height are 25.3 mm and 49 mm, respectively. This containment ring has a straight path (C) of diameter 3 mm and a conical cut (D). Incident X-rays can travel through the straight path and irradiate the sample. The conical cut is for the passage of transmitted and diffracted X-rays, whose maximum 2θ is 10° . The culet diameter of the anvil is 3 mm. We tested anvils with tapering angles (α) of 20, 25 and 30° . In the present study we mainly used anvils with a tapering angle of 20° . The outer diameter and the height of the anvils are both 25 mm. The side wall of the anvil is surrounded by a polyimide tape (Kapton) of thickness 0.13 mm for electrical insulation. The top and

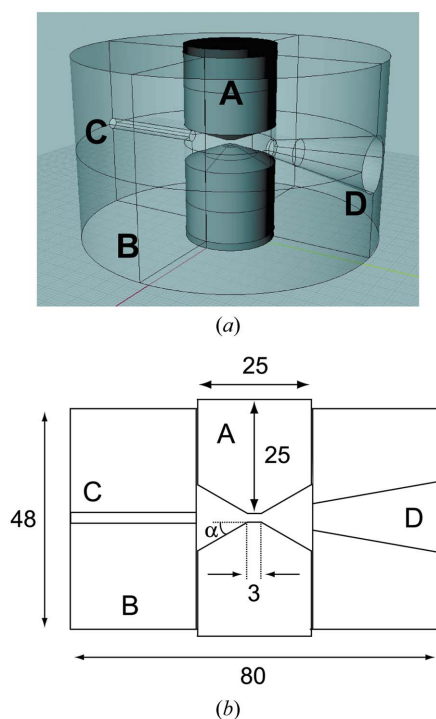


Figure 1 Schematic three-dimensional illustration (a) and a cross section (b) of the Drickamer cell. A, tungsten carbide anvils; B, cylinder (tool-steel); C, straight path (3 mm diameter); D, conical cut; α , taper angle (20° , 25° and 30°).

bottom surface of the containment ring are also covered by the polyimide tape for electrical insulation. This Drickamer cell can be compressed using any uniaxial hydraulic press as long as the cell can fit. In the present study we used the D-DIA module and the 250 ton press installed in the GSECARS bending-magnet station, 13-BM-D, at the Advanced Photon Source (Argonne, IL, USA) (Wang *et al.*, 2003). The D-DIA module has two conical cuts in the X-ray directions which let us carry out X-ray diffraction experiments using monochromatic X-rays under high pressure. By removing the four side anvils in the D-DIA, we used a vertical pair of anvils made of WC to compress the Drickamer cell.

2.2. Sample assembly

Fig. 2 shows a schematic illustration of the cell assembly. We used an outer plastic cylinder (B), which is made of the plastic material PEEK (supplied by NIPPON POLYPENCO; see Yamazaki & Karato, 2001), to align all the parts inside. The inner parts (C) are made of pyrophyllite (raw), which was machined using a CNC milling machine. We employed a gasket (D) made of another type of plastic, PBI (NIPPON POLYPENCO, outer diameter 20 mm, inner diameter 5 mm, thickness 0.8 mm). This material has some advantages for radial X-ray diffraction experiments under high pressure: high strength, high hardness and high X-ray transparency (Take-shita & Terakura, 2004). These plastic materials are stably used even at high temperature up to 550 K under 0.1 MPa. The pressure medium (E) was made of amorphous boron powder mixed with epoxy resin (4:1 by weight), with a hole of 1.5 mm diameter as the sample chamber. We used two kinds of samples (H): a polycrystalline platinum rod of diameter 0.3 mm, and polycrystalline sintered Mg_2SiO_4 ringwoodite of

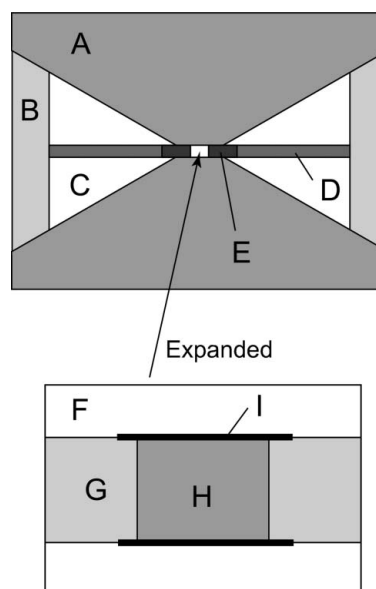


Figure 2 Schematic illustrations of the cell assembly. A, tungsten carbide anvil; B, outer plastic cylinder (PEEK); C, pyrophyllite cap; D, plastic gasket (PBI); E, pressure medium (boron powder + epoxy resin); F, pyrophyllite disc; G, sample capsule (graphite); H, polycrystalline sample; I, gold foil.

diameter 0.5 mm. The latter was synthesized at 20 GPa and 1523 K using a Kawai-type multi-anvil apparatus, Orange-3000, installed at the Geodynamics Research Center, Ehime University. The length of both samples was 0.3 mm. The samples were embedded in a graphite capsule (G). Pyrophyllite discs (F) were placed just below and above the sample. In the run for ringwoodite, gold foils of thickness 2 μm (I) were placed in between the sample and the discs as strain markers.

2.3. Experimental set-up with monochromatic X-rays

Fig. 3 shows a top view of the experimental set-up in the GSECARS bending-magnet beamline, 13-BM-D. This set-up is very similar to that of D-DIA experiments using monochromatic X-rays (e.g. Uchida *et al.*, 2004; Nishiyama *et al.*, 2007). White X-rays from the bending magnet were monochromated at an energy of 65 keV (wavelength = 0.191 \AA) by a double-crystal Si(111) monochromator. WC front slits (B) were used to collimate a fine beam (0.05 mm vertical; 0.1 mm horizontal) for X-ray diffraction. Incident X-rays passed through the straight path of the containment ring in the Drickamer cell and irradiated the sample between the anvils. The conical cut of the containment ring made it possible to observe diffraction Debye rings over the entire 360° detector azimuth range, perpendicular to the incident beam direction (J). Radial X-ray diffraction patterns thus obtained were used to calculate hydrostatic pressure and differential stress (e.g. Singh, 1993; Merkel *et al.*, 2002). Two-dimensional X-ray diffraction patterns were recorded using an X-ray charge-coupled device (CCD) detector, Mar-165 (K). The detector orientation relative to the incident beam was calibrated using a diffraction standard (CeO_2). The sample-to-detector distance was determined by matching the observed ambient d values of the sample inside the Drickamer cell with those of references: in the case of ringwoodite, we used data reported by Sasaki *et al.* (1982); in the case of platinum, JCPDS data were used. The typical sample-to-detector distance was

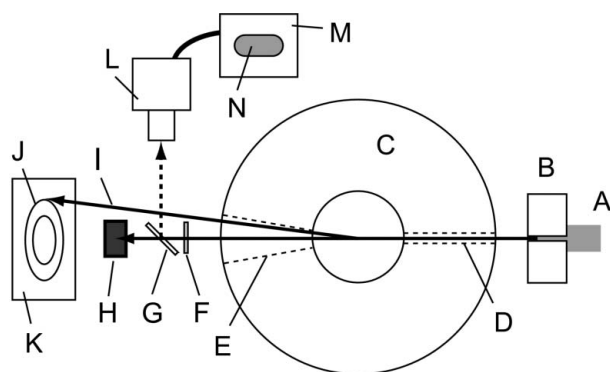


Figure 3 Schematic illustration of the top view of the experimental set-up in the GSECARS bending-magnet beamline, 13-BM-D. A, incident monochromatic X-rays (65 keV); B, front slits; C, cylinder; D, straight path; E, conical cut; F, YAG phosphor; G, mirror; H, beam stop (Pb); I, diffracted X-rays; J, Debye ring; K, two-dimensional X-ray CCD; L, CCD camera; M, PC monitor; N, radiographic image.

350 mm. The relation between the sample-to-detector distance and the diameter of the sample can cause artificial broadening of diffraction peaks. In the case of the ringwoodite sample (0.5 mm diameter), the sample size causes 0.004° error ($2\theta = 5^\circ$), which is smaller than that caused by one pixel difference on the X-ray CCD detector (0.01°). Therefore, the effect of this artificial broadening is not significant in the present study. The front slits can be moved out of the beam path, providing a wider beam (1.5 mm vertical; 2.0 mm horizontal) for X-ray radiography. Transmitted X-rays irradiated the YAG phosphor screen (F) which converted X-ray contrast to visible light. The visible image on the mirror (G) was recorded using a CCD camera (L) connected to a PC. Radiographic images of the sample (N) were then analyzed and the total axial strains of the sample were calculated using the sample length.

3. Results and discussion

3.1. X-ray diffraction measurements

Fig. 4(a) shows an example of a two-dimensional X-ray diffraction pattern of polycrystalline ringwoodite obtained under high pressure. We can clearly observe diffraction peaks from ringwoodite up to the 440 reflection. One diffraction peak of graphite (002 reflection) can also be seen because

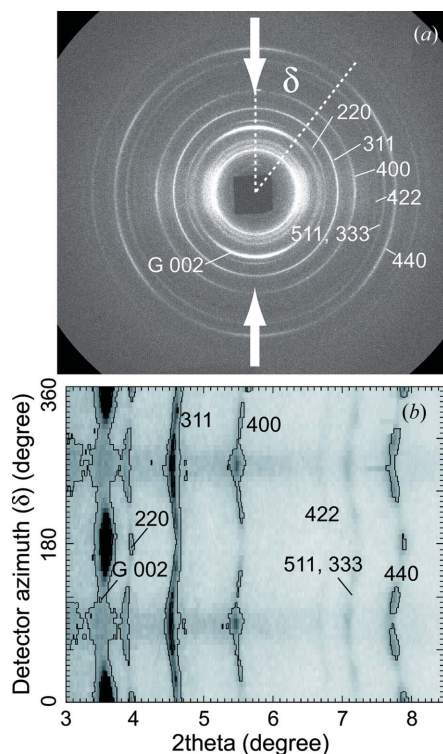


Figure 4 Example of a two-dimensional X-ray diffraction pattern of polycrystalline ringwoodite obtained under high pressure (a). G002 represents a diffraction peak of graphite (002 reflection) and other numbers represent indices of diffraction peaks of ringwoodite. The pair of arrows show the compression directions. The converted pattern of (a) from the original form in polar coordinates into the Cartesian system is also shown (b). We can clearly see the detector azimuth angle (δ) dependence of 2θ for all the diffraction peaks of ringwoodite observed in this pattern.

graphite was used as the sample capsule. The arrows show the direction of compression.

Fig. 4(b) shows the converted pattern of Fig. 4(a) from the original form in polar coordinates into the Cartesian system, where the horizontal and vertical axes are 2θ and detector azimuth δ ($\delta = 0$ is parallel to the compression axis), respectively, with intensity represented by darkness. Under perfect hydrostatic conditions the centroid of each diffraction peak exhibits no dependence on the azimuth angle, resulting in a straight line in this plot. Under a differential stress field, however, centroids of the diffraction lines show a clear dependence on δ . The maximum 2θ values for the peaks are at $\delta \simeq 0^\circ$ and 180° , corresponding to the direction parallel to the compression axis, whereas the minimum 2θ values are observed at $\delta \simeq 90^\circ$ and 270° , parallel to radial directions and perpendicular to the compression axis. In order to create diffraction patterns with Cartesian systems and to analyze the azimuth dependence of peak positions, we used the software package *saxs15id*, developed at ChemMatCARS, University of Chicago (Cookson *et al.*, 2006) (the software package is available at <http://cars.uchicago.edu/chemmat/>). A Gaussian function was employed to determine the centroid of each diffraction peak. Intensity variations as a function of azimuth angle δ are also observed. For example, intensities of the 220 and 440 peaks show maxima at $\delta = 0, 60, 120, 180, 240$ and 300° with a well developed sixfold symmetry. These observations are completely consistent with those in previous studies (Nishiyama *et al.*, 2005; Wenk *et al.*, 2005), suggesting that the deformation is dominated by the $\{111\}\langle\bar{1}10\rangle$ slip system (Wenk *et al.*, 2005). Intensity variation information as a function of δ is also useful for estimating the dominant slip system of deformation (*e.g.* Merkel *et al.*, 2002).

Using the diffraction patterns thus obtained, hydrostatic pressure and differential stress can be calculated (*e.g.* Duffy *et al.*, 1999; Merkel *et al.*, 2005). The measured d -spacing, $d_m(hkl)$, can be fitted by the following equation,

$$d_m(hkl) = d_p(hkl)[1 + (1 - 3 \cos^2 \chi)Q(hkl)], \quad (1)$$

where χ is the true azimuth angle given by $\cos \chi = \cos \theta \cos \delta$, and $d_p(hkl)$ is the d -spacing under the equivalent hydrostatic pressure. $d_p(hkl)$ is determined at $\chi = 54.7^\circ$ and symmetrically equivalent angles, where $(1 - 3 \cos^2 \chi) = 0$. Hydrostatic pressure is then calculated using the $d_p(hkl)$ information of available reflections and the equation of state of the sample. We can also evaluate differential stress [$t = \sigma_a - \sigma_r$, where σ_a and σ_r are stresses in the axial (vertical) and radial (horizontal) directions of the sample, respectively]: $t(hkl) = 6Q(hkl)G(hkl)$, where $G(hkl)$ is the appropriate modulus of the aggregate, which is calculated using single-crystal elastic moduli (Weidner *et al.*, 2004; Merkel *et al.*, 2005).

Fig. 5 shows an example of analysis to evaluate hydrostatic pressure and differential stress using the 311 reflection of Mg_2SiO_4 ringwoodite. The diffraction pattern was collected at 20 tons. $d_m(311)$ varies with true azimuth (χ), which indicates that the sample is under a uniaxial stress field. The bold line represents the result of a least-squares fit of $d_m(311)$ to equation (1). The determined $d_p(311)$ and $Q(311)$ are

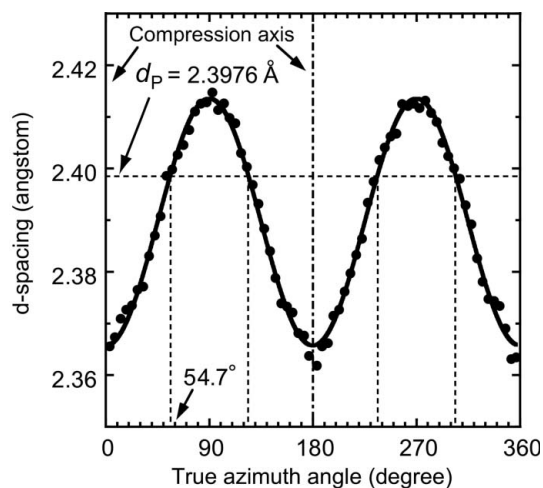


Figure 5

Example of true azimuth angle (χ) dependence of d -spacing of the 311 reflection of ringwoodite. The bold line represents the result of a least-squares fit of $d_m(311)$ to equation (1) (see text). The determined $d_p(311)$ and $Q(311)$ are 2.3976 Å and 0.00665, respectively. We calculated the hydrostatic pressure and $t(311)$ as 8.2 GPa and 5.0 GPa, respectively. Errors of these plots in the vertical axis are smaller than the size of the symbols.

2.3976 Å and 0.00665, respectively. Using these two parameters, we calculated the hydrostatic pressure and differential stress [$t(311)$] as 8.2 GPa and 5.0 GPa, respectively.

Fig. 6 shows the relation between applied load and generated hydrostatic pressure. Using the present experimental setup, pressures up to 32 GPa can be generated at a load of 95 tons. Up to about 20 GPa (a load of about 40 tons), pressure increases linearly with applied load. Above this pressure, the relation between pressure and applied load becomes non-linear and pressure generation efficiency decreases with applied load. The pressure generation curve obtained in the run on a platinum sample, using anvils with a tapering angle of 20° , is quite similar to that on a ringwoodite sample with a

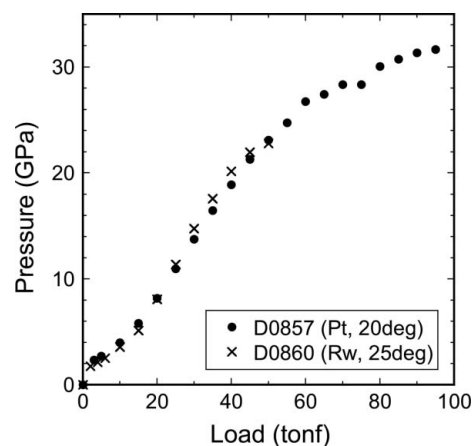


Figure 6

Relation between applied load and generated hydrostatic pressure. Solid circles and crosses represent data obtained in the run of platinum (anvil taper angle, 20°) and ringwoodite (anvil taper angle, 25°), respectively. A pressure of 32 GPa was generated for a load of 95 tons. Note that pressure increases linearly with applied load up to about 20 GPa (40 tons) and the P versus L relation becomes non-linear above this pressure.

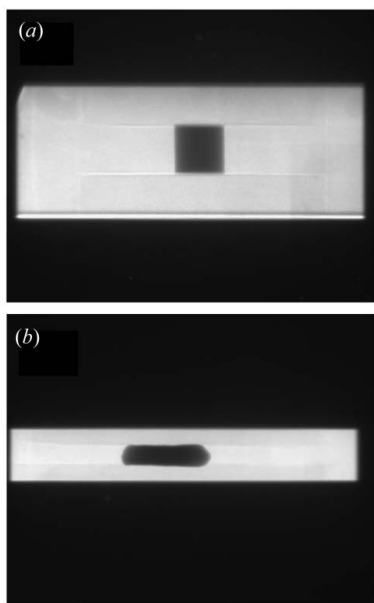


Figure 7
Example of X-ray radiographs taken in the run of the platinum sample, (a) before compression, (b) at 40 tons ($P \simeq 20$ GPa). We can clearly see that the sample deforms by applying a load. The length of the sample was shortened and the diameter was enlarged after the compression.

tapering angle of 25° , which might indicate that the effect of the taper angle of anvils to pressure generation efficiency is small. Further details of these runs will be reported in separate papers.

3.2. X-ray radiography measurements

Fig. 7 shows examples of X-ray radiographs of the platinum sample at 0 ton (Fig. 7a) and 40 tons (Fig. 7b). We can clearly see that the sample deforms by applying a load. In these radiographs the upper and lower boundaries between the bright and dark areas represent culet surfaces of the upper and lower anvils. The distance between the anvils at a pressure of about 20 GPa (40 tons) is about one-third of that under ambient conditions.

We can determine the axial sample length using the radiographs and calculate the total axial strain: $\epsilon_{\text{total}} = (l_0 - l)/l_0$, where l is the sample length under pressure and l_0 is the reference length before compression. Fig. 8 shows changes of sample length and total axial strain as a function pressure. The sample length decreases with pressure. The slope of the length–pressure curve becomes more gentle with increasing pressure. The total axial strain reaches 55% at 19 GPa and the curve shows saturation above this pressure. Note that the pressure where the length–pressure curve reaches saturation is close to where the load–pressure curve (Fig. 6) starts to show non-linearity.

3.3. Advantages of sintered diamond anvils

We also tested the use of sintered diamond anvils in an effort to push deformation experiments to higher pressures. Fig. 9 shows a schematic illustration of a composite anvil

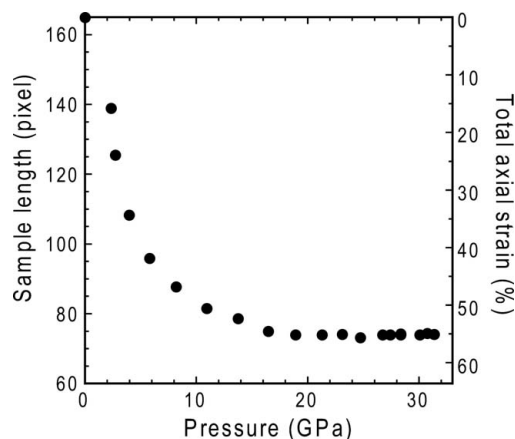


Figure 8
Changes of the sample length and total axial strain of platinum as a function of pressure. The total axial strain reaches about 55% at a pressure of 19 GPa and the curve shows saturation above this pressure.

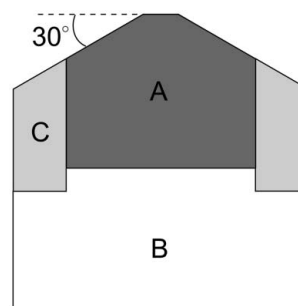


Figure 9
Schematic illustration of a composite anvil system with sintered diamond anvil. A, sintered diamond anvil; B, tungsten carbide anvil backup; C, stainless steel ring.

system with a sintered diamond anvil developed in the present study. This composite design reduces the volume of the sintered diamond, thereby saving the cost of experiments. We used a sintered diamond anvil made by Tomei Diamond Co. Ltd with a diameter of 16 mm and height of 10 mm (A). The culet diameter and tapering angle are 3 mm and 30° , respectively. The sintered diamond anvil was embedded into a stainless steel ring (B). We employed an anvil backup made of WC whose material is the same as that used for anvils (see Fig. 1 and text).

Sodium chloride was used as a sample in this test. Fig. 10 shows a comparison between a two-dimensional X-ray diffraction pattern obtained in the run for platinum using WC anvils and that using the sintered diamond anvil. Both diffraction patterns were collected at pressures of about 27 GPa. In the case of the run for platinum (Fig. 10a), a large portion of the Debye rings are blocked by WC anvils because the anvil gap becomes narrower at high pressure (see Fig. 7). This makes the evaluation of stress and pressure difficult. We can observe non-interrupted Debye rings only up to 5.5° in 2θ , limiting the number of diffraction peaks which can be used for these analyses. On the other hand, in the case of sintered diamond anvils, we can clearly observe continuous Debye rings up to 10° in 2θ , which is the maximum 2θ angle we

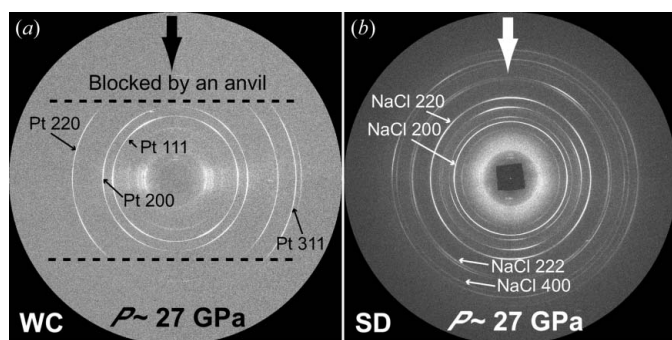


Figure 10

Comparison between the two-dimensional X-ray diffraction pattern obtained using WC anvils (a) and that using sintered diamond anvils (b). The bold arrows show the compression directions. In (a), the upper and lower parts of the Debye rings are blocked by WC anvils. In (b), the entire Debye rings are observed because of high X-ray transparency of the sintered diamond anvils.

defined in the Drickamer apparatus, making it possible to analyze a large number of diffraction peaks to evaluate hydrostatic pressure and differential stress. Because of high X-ray transparency of this material (Co content is 7.5 vol%), diffracted X-rays (65 keV) can be easily detected through the sintered diamond anvils. The use of sintered diamond anvils has a significant advantage for stress measurements using the Drickamer apparatus.

We thank T. Yagi and H. Gotou for constructive comments. We also thank N. Lazarz, F. Sopron, M. Jagger and N. Hilairt for their support during the experiment at 13-BM-D at GSECARS, University of Chicago. We are grateful to Y. Higo for cooperation for developing software to reduce X-ray radiographs for determining macroscopic sample strains. This work was performed at GeoSoilEnviroCARS (Sector 13), Advanced Photon Source, Argonne National Laboratory. GeoSoilEnviroCARS is supported by the National Science Foundation – Earth Sciences (EAR-0622171) and Department of Energy – Geosciences (DE-FG02-94ER14466). Use of the Advanced Photon Source was supported by the US Department of Energy, Office of Science, Office of Basic Energy Sciences, under Contract No. DE-AC02-06CH11357. This work was partially supported by NSF grant EAR0652574. This

work was also supported by a Grant-in-Aid for Young Scientists (Start-up) to NN (No. 19840033).

References

- Balchan, A. S. & Drickamer, H. G. (1961). *Rev. Sci. Instrum.* **32**, 308–313.
- Cookson, D., Kirby, N., Knott, R., Lee, M. & Schultz, D. (2006). *J. Synchrotron Rad.* **13**, 440–444.
- Duffy, T. S., Hemley, R. J. & Mao, H. K. (1995). *Phys. Rev. Lett.* **71**, 1371–1374.
- Duffy, T. S., Shen, G., Heinz, D. L., Shu, J., Ma, Y., Mao, H. K. & Hemley, R. J. (1999). *Phys. Rev. B*, **60**, 15063–15073.
- Funamori, N. & Yagi, T. (1993). *Geophys. Res. Lett.* **20**, 387–390.
- Funamori, N., Yagi, T. & Uchida, T. (1994). *J. Appl. Phys.* **75**, 4327–4331.
- Gotou, H., Yagi, T., Frost, D. J. & Rubie, D. C. (2006). *Rev. Sci. Instrum.* **77**, 035113.
- Kinsland, G. L. & Bassett, W. A. (1977). *J. Appl. Phys.* **48**, 978–985.
- Mao, H. K., Shu, K. J., Shen, G., Hemley, R. J., Li, B. & Singh, A. K. (1998). *Nature (London)*, **396**, 741–743.
- Meade, C. & Jeanloz, R. (1988). *J. Geophys. Res.* **93**, 3261–3269.
- Merkel, S., McNamara, A. K., Kubo, A., Speziale, S., Miyagi, L., Meng, Y., Duffy, T. S. & Wenk, H. R. (2007). *Science*, **316**, 1729–1732.
- Merkel, S., Shu, J., Gillet, P., Mao, H. K. & Hemley, R. J. (2005). *J. Geophys. Res.* **110**, B05201.
- Merkel, S., Wenk, H. R., Shu, J., Shen, G., Gillet, P., Mao, H. K. & Hemley, R. J. (2002). *J. Geophys. Res.* **107**, 2271.
- Nishiyama, N., Wang, Y., Rivers, M. L., Sutton, S. R. & Cookson, D. (2007). *Geophys. Res. Lett.* **34**, L23304.
- Nishiyama, N., Wang, Y., Uchida, T., Irifune, T., Rivers, M. L. & Sutton, S. R. (2005). *Geophys. Res. Lett.* **32**, L04307.
- Sasaki, S., Prewitt, C. T., Sato, Y. & Ito, E. (1982). *J. Geophys. Res.* **87**, 7829–7832.
- Singh, A. K. (1993). *J. Appl. Phys.* **73**, 4278–4286.
- Takeshita, N. & Terakura, C. (2004). *Rev. High Press. Sci. Tech.* **14**, 260–264. (In Japanese.)
- Uchida, T., Wang, Y., Rivers, M. L. & Sutton, S. R. (2004). *Earth Planet. Sci. Lett.* **226**, 117–126.
- Wang, Y., Durham, W. B., Getting, I. C. & Weidner, D. J. (2003). *Rev. Sci. Instrum.* **74**, 3002–3011.
- Weidner, D. J., Li, L., Davis, M. & Chen, J. (2004). *Geophys. Res. Lett.* **31**, L06621.
- Wenk, H. R., Ischia, G., Nishiyama, N., Wang, Y. & Uchida, T. (2005). *Phys. Earth Planet. Int.* **152**, 191–199.
- Wenk, H. R., Matthies, S., Hemley, R. J., Mao, H. K. & Shu, J. (2000). *Nature (London)*, **405**, 1044–1047.
- Yagi, T., Utsumi, W., Yamakata, M., Kikegawa, T. & Shimomura, O. (1992). *Phys. Rev. B*, **46**, 6031–6039.
- Yamazaki, D. & Karato, S. (2001). *Rev. Sci. Instrum.* **72**, 4207–4211.